

Optimization of Mg–Al Layered Double Hydroxide Film Preparation and Corrosion Resistance Study on AZ91D Mg Alloy by Multivariate Polynomial Regression Fitting

Chengfeng Wang, Bofan Liu, Pengxu Wei, Kepei Xie, Yu Chen, Meifeng Wang, Xiaoqing Du,* and Dongchu Chen*

Cite This: *ACS Omega* 2024, 9, 19158–19168

Read Online

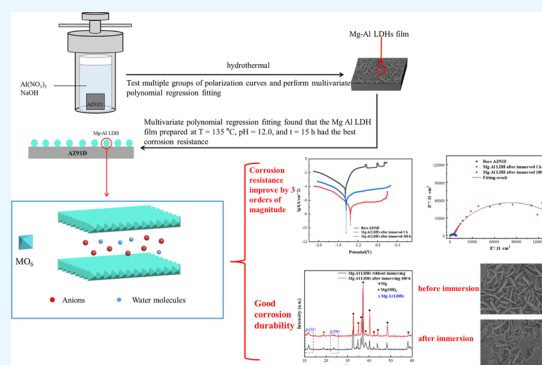
ACCESS |

Metrics & More

Article Recommendations

Supporting Information

ABSTRACT: Layered double hydroxide (LDH) films have received extensive attention for their unique physical barrier function and ion exchange properties, which make them promising candidates for corrosion protection of magnesium alloys. In this paper, we used the multiple polynomial regression fitting method to establish a regression equation for the electrochemical corrosion resistance with the reaction temperature (T), pH, and reaction time (t) of the Mg–Al LDH film on the AZ91D magnesium alloy. The goodness of fit, confidence, and residual analyses confirmed the high accuracy of the model equation. According to the calculation using the f_{mincon} function, the best corrosion resistance of the prepared samples could be achieved when the parameters are $T = 135\text{ }^{\circ}\text{C}$, $\text{pH} = 12.0$, and $t = 15\text{ h}$. Then, the experimental results showed that the corrosion current density (I_{corr}) of the obtained LDH film under the above conditions could be $1.07 \times 10^{-7}\text{ A/cm}^2$, approximately 3 orders of magnitude lower than the magnesium alloy substrate, after immersion in a 3.5 wt % NaCl solution for 180 h, the surface structure of the LDH film did not change significantly, and the I_{corr} was still 2 orders of magnitude higher than that of the magnesium alloy substrate. Hence, a synergistic effect equation for the reaction temperature, pH, and reaction time on the corrosion resistance of the LDH film on a magnesium alloy surface prepared by the hydrothermal method was obtained. Moreover, using this equation, we obtained an LDH film with good corrosion resistance and durability, providing theoretical guidance for optimizing the process of preparing the LDH film by the hydrothermal method in practical applications.



1. INTRODUCTION

Magnesium (Mg) alloys have attracted extensive attention due to their low density and good mechanical properties.^{1–3} However, the poor corrosion resistance of magnesium alloys tremendously hinders their widespread application.⁴ To improve the corrosion resistance of magnesium alloys, surface treatment methods are usually used to build protective coatings on the surfaces of magnesium alloys, for instance, heat treatment,⁵ chemical conversion coatings,⁶ anodic oxide coatings,⁷ electroplating coating,⁸ electroless coating,⁹ vapor deposition,¹⁰ etc. Among these, chemical conversion coating has attracted worldwide attention due to its simple preparation process and its ability to handle workpieces with complex shapes.^{6,11} The layered double hydroxide (LDH) film in chemical conversion films is favored by researchers due to its simple preparation process, environmental protection, and good corrosion resistance.^{12,13}

LDH is a general term for hydrotalcite and hydrotalcite-like compounds. LDH consists of a cationic host layer of divalent and trivalent cations and an anionic layer of organic or inorganic anions, and it can be represented by the general formula

$[\text{M}_{1-x}^{2+}\text{M}_x^{3+}(\text{OH})_2]^{x+}(\text{A}^{n-})_{x/n} \cdot m\text{H}_2\text{O}$. In the formula, M^{2+} and M^{3+} represent cations occupying octahedral pores in layered layers, A^{n-} represents the interlayer charge compensation anion, n is the charge of the intercalated anion, m is the number of water molecules. X is the molar ratio of $\text{M}^{3+}/(\text{M}^{2+} + \text{M}^{3+})$, which generally ranges from 0.20 to 0.33. LDH has a brucite-like ($\text{Mg}(\text{OH})_2$) intercalated structure, and isomorphous replacement of trivalent cations for a fraction of divalent cations leads to the positively charged host layers, in which each metal cation M^{2+} or M^{3+} is coordinated by six oxygen atoms, forming the $\text{M}^{2+}/\text{M}^{3+}(\text{OH})_6$ octahedron. These octahedra constitute the two-dimensional sheets via edge sharing, which then stack together by hydrogen bonding between the hydroxyl groups of

Received: December 23, 2023

Revised: April 8, 2024

Accepted: April 10, 2024

Published: April 19, 2024



adjacent sheets, balanced by a wide range of interlayer anions A^{n-} . The entire LDH structure is usually electrically neutral.^{14,15} The anions between LDH laminates can be chemically modified based on the anion-exchange mechanism. Generally, high-valence anions are easier to exchange with low-valence anions.¹⁶ Therefore, LDH films can provide excellent physical barrier protection on the surface of magnesium alloys. At the same time, the unique interlayer anion exchangeability of LDH allows it to capture corrosive anions, significantly improving the corrosion resistance of magnesium alloys.^{15–18}

LDH films can be prepared on the surface of magnesium alloys by coprecipitation, electrochemical deposition, and hydrothermal methods.^{14–21} Among them, LDH films prepared by hydrothermal processes have dense structures, excellent adhesion to the substrate, and good corrosion resistance. Kamiyama et al.²⁰ and Chen et al.²¹ researched the effect of different reaction times at specific temperatures and pH on the corrosion resistance of the prepared LDH film and ultimately found the optimal reaction time. However, they did not consider the effects of temperature and pH. Lin et al.²⁴ found through a series of studies that alkaline environments are more conducive to the growth of LDH films and also explored the effect of reaction time at pH = 11.5 on films' growth and corrosion resistance; Chen et al.²⁴ further investigated the effects of time, temperature, and pH on the corrosion resistance of LDH films through a single-factor experimental method. The corrosion resistance of the LDH films formed at low values of pH or high temperatures or short treatment time is deteriorative. Previous studies have shown that the corrosion resistance of LDH films prepared by the hydrothermal method is greatly affected by the reaction temperature, pH, and reaction time. However, most previous studies explored the impact of various preparation parameters focusing on single-factor experimental methods, without considering the interaction and synergistic effects among multiple factors.^{20–25} Although the orthogonal experiment can establish an analytical model for the impact of multiple independent variables on dependent variables, exploring the impact of the relationship between independent variables on the dependent variable is challenging and is further limited by its ability to depict only linear relationships between the factors and corresponding variables. Therefore, it is necessary to establish more complex nonlinear models to clarify the internal synergistic effects between the influencing factors to obtain better corrosion-resistant LDH films.

The field of metal corrosion relies on fundamental data, but dealing with the extensive and intricate data related to the corrosion resistance of materials can be challenging due to its high volume and complexity.²⁶ In order to explore the connection between variables (such as dependent and independent variables) in the context of corrosion, it is essential to carefully analyze and uncover the underlying mechanism within the collected corrosion data. The goal is to create a specific or conceptual mathematical model that can be used for predicting future outcomes related to corrosion. Multiple linear regression refers to the establishment of a mathematical model and making predictions through correlation analysis of two or more independent variables and one dependent variable. This method can eliminate the correlation between variables and reduce the screening process conditions. It can also provide a deeper understanding of the interaction between different dependent variables and deduce the optimal combination of dependent variables in the case of limited data, thus significantly saving time and cost of research.²⁷ In 1971, Haynie et al.²⁸

proposed an atmospheric corrosion model for carbon steel based on multivariate linear equations for corrosion rate vs SO_2 concentration, exposure time, and total oxide thickness. Zor et al.²⁹ investigated the optimal process conditions for galvanizing stainless steel surfaces by varying three independent variables: stirring speed, bath temperature, and plating time to obtain different zinc layers. They then tested the corresponding samples' potential dynamic polarization curves to get the corrosion current density as the dependent variable. Wang et al. successfully established the relationship between the three independent and dependent variables and deduced the quadratic regression equation to predict the optimal process conditions.³⁰ They examined how different electrolyte parameters affected corrosion resistance by employing statistical techniques. They established the variance and Pareto of the regression equation of corrosion current density. The analysis was conducted using a combination design of orthogonal rotation based on a ternary quadratic regression.

Therefore, utilizing a multiple linear regression equation is a promising approach for assessing the impact of process conditions on the corrosion resistance of the samples. Additionally, optimization of the process parameters can be achieved through the application of this regression equation.

In this paper, Mg–Al LDH films were *in situ* prepared on an AZ91D magnesium alloy by the hydrothermal method. The magnesium alloy was immersed in an alkaline aluminum nitrate solution with varying pH values, reacted at various temperatures, and lasted for different times; finally, LDH films successfully formed on the magnesium alloy samples. Then, a high-precision mathematical model was deduced and fitted to explore the synergistic effect of reaction temperature, pH, and reaction time on the corrosion resistance of the LDH film prepared on the magnesium alloy surface by the hydrothermal method. The accuracy of the equation is also verified based on the confidence interval and goodness of fit. Meanwhile, the high-precision mathematical model was also used to predict the best process conditions for the elaboration of corrosion-resistant film based on experimental data. Eventually, the LDH films obtained under the predicted best process conditions were systematically studied using scanning electron microscopy (SEM), X-ray diffraction (XRD), Fourier transform infrared spectroscopy (FT-IR), electrochemical testing, as well as long-term immersion experiments.

2. EXPERIMENT AND CHARACTERIZATION

2.1. Experimental Materials. Mg–Al LDH films were prepared *in situ* on an AZ91D magnesium alloy substrate. The composition of the AZ91D magnesium alloy substrate is Al of 8.5–9.5 wt %, Zn of 0.45–0.9 wt %, Mn of 0.17–0.4 wt %, Si < 0.08 wt %, Fe < 0.004 wt %, and Ni < 0.001 wt %, with balance being Mg. AZ91D magnesium alloy was cut into 30 mm × 30 mm × 0.5 mm as a working sample for subsequent processing. The analytically pure grade aluminum nitrate ($Al(NO_3)_3 \cdot 9H_2O$, 99%), sodium chloride (NaCl, 99%), and sodium hydroxide (NaOH, 99%) were all purchased from Beijing Inno Chem Science & Technology Co. The solvent used for all solutions in this article was deionized water ($18.2 M\Omega\text{ cm}^{-1}$).

2.2. Preparation of Mg–Al LDH Films. The AZ91D magnesium alloy was grounded successively with 200, 400, 800, 1200, and 2000-grit SiC sandpaper and then ultrasonically cleaned in absolute ethanol for 10 min. Subsequently, the magnesium alloy was immersed in a 2 M NaOH solution to remove surface oxides through ultrasonic cleaning for 1 min and

then ultrasonically cleaned in ethanol for 10 min. Finally, the magnesium alloy was taken out and dried in cold air for further use.

0.05 M $\text{Al}(\text{NO}_3)_3 \cdot 9\text{H}_2\text{O}$ (0.05 M) was dissolved in deionized water, and 4 M NaOH was added to adjust the solution pH. Subsequently, the obtained solution and the pretreated magnesium alloy sample were transferred to a hydrothermal reactor and reacted at a particular temperature for different times. Then, the samples were removed and washed with deionized water. Finally, the sample was dried with cold air.

2.3. Characterization. Scanning electron microscopy (SEM) was used to characterize the surface and cross-sectional morphology of the samples. SEM test was conducted on S-4800 produced by HITACHI. All samples for SEM characterization were sprayed with gold for 60 s for good conductivity before testing. The IncaEnergyX-Max20 energy-dispersive spectrometer (EDS) produced by Oxford was used to determine the elemental composition of the film. The structure of the film was characterized by X-ray diffraction (XRD). The XRD test was carried out on the Smart lab produced by Rigaku. The target material was Cu; the scanning range was $5\text{--}80^\circ$, and the scanning speed was $5^\circ/\text{min}$. The XRD pattern was analyzed by MDI Jade 6 software. Fourier transform infrared spectroscopy (FT-IR) was used to characterize the distinct functional groups of the film. The FT-IR test was conducted on a Nicolet iS50 produced by Thermo Scientific with the ATR method and air as the background. The scanning range was $400\text{--}4000\text{ cm}^{-1}$.

The corrosion resistance of the samples was evaluated by the potentiodynamic polarization curve and electrochemical impedance spectroscopy (EIS). The potentiostat was CS2350H manufactured by Wuhan Corrtest. A typical three-electrode system was used, in which magnesium alloy was the working electrode (test area 1 cm^2) and platinum sheet ($2\text{ cm} \times 2\text{ cm}$) and saturated calomel electrode (SCE, $E = +0.24\text{ V}$ vs SHE) as the counter electrode and the reference electrode, respectively. All electrochemical tests were conducted in the Faraday cage. Before the test, the working electrode was immersed in 3.5 wt % NaCl solution for 1 h until the open circuit potential (OCP) becomes stable. The potentiodynamic polarization test started from $-0.5\text{ V} \sim E_{\text{ocp}} + 1\text{ V}$, and the scanning rate was 5 mV/s . All samples were tested at room temperature ($25 \pm 2\text{ }^\circ\text{C}$). The EIS is also tested when the open circuit potential is stable. The test frequency range was 100 kHz to 100 mHz, and the disturbance potential (AC) was 10 mV. The EIS is analyzed and fitted using Z-View software to obtain the corresponding electrochemical parameters. All experiments were repeated three times for reproducibility.

The immersion experiment was conducted at $25\text{ }^\circ\text{C}$.

2.4. Fitting Procedure. As the self-corrosion current density reflects the corrosion rate of the entire system after the coupling of the LDH film and substrate, while reaction resistance in EIS only reflects the corrosion rate of the magnesium alloy substrate, the corrosion condition of the LDH film needs to be considered in the actual service environment. Therefore, the self-corrosion current density in the polarization curve is used to characterize the corrosion resistance of the LDH film in this modeling. The data were fitted using the regress function of MATLAB. Subsequently, the confidence intervals for the fitted coefficients and residuals were output using the regress function and built-in functions. The fitted results were used to find the most value in the interval using the fmincon function. Finally, the residuals were calculated by the rcoplot function.

3. REGRESSION ANALYSIS

Linear regression is a commonly used data model.

Let an n -dimensional independent variable be

$$\mathbf{X} = (x_1, x_2, \dots, x_n)^T \quad (1)$$

The one-dimensional dependent variable is

$$\mathbf{y} = (y_1, y_2, \dots, y_n)^T \quad (2)$$

If a piece of data has n attributes, the matrix form of multiple linear regression is

$$\mathbf{f}(\mathbf{X}) = \mathbf{w}^T \mathbf{X} + b \quad (3)$$

Among them,

$$\mathbf{w} = (w_1, w_2, \dots, w_n)^T \quad (4)$$

$$\mathbf{b} = (b_1, b_2, \dots, b_n)^T \quad (5)$$

Traditional linear regression is used to study the relationship between a dependent variable and an independent variable. When dealing with the relationship between a dependent variable and multiple independent variables, we typically employ polynomial regression. According to the Taylor formula, if the function $f(x)$ is differentiable at x_0 , the constant in the neighborhood $U(x_0)$ remains constant:

$$f(x) = \sum_{k=n}^n \frac{f^{(k)}(x_0)(x-x_0)^k}{k!} + R_n(x) \quad (6)$$

Among them,

$$R_n(x) = \frac{f^{(n+1)}(\varepsilon)}{(n+1)!} (x-x_0)^{n+1} \quad (7)$$

Here, ε is the value between x and x_0 . In this formula,

$$P_n(x) = \sum_{k=n}^n \frac{f^{(k)}(x_0)(x-x_0)^k}{k!} \quad (8)$$

This formula represents the n th-order Taylor polynomial of function $f(x)$, where $R_n(x)$ is the error between $P_n(x)$ and $f(x)$, also referred to as the n -order Taylor remainder.

If the derivative of order $(n+1)$ of function $f(x)$ has an upper bound M in the neighborhood $U(x_0)$

$$\lim_{x \rightarrow x_0} \left| \frac{R_n(x)}{(x-x_0)^n} \right| \leq \lim_{x \rightarrow x_0} \frac{M}{(n+1)!} |x-x_0| = 0 \quad (9)$$

Therefore, this is

$$R_n(x) = o((x-x_0)^n) \quad (10)$$

The geometric interpretation of the Taylor formula involves approximating the original function using a polynomial function. Because the polynomial function can be differentiated at any point, it is easy to calculate and convenient for finding extreme values and determining the nature of functions. Consequently, the Taylor formula can be used as a reliable tool for obtaining information about functions and approximating their properties.

The preceding section is an introduction to the Taylor formula for univariate functions. This formula can also be extended to multivariate functions. In this article, only the second-order multivariate Taylor formula is used. Therefore, only the matrix form of the second-order Taylor formula for multivariate functions is presented here:³¹

$$f(\mathbf{X}) = f(\mathbf{X}_k) + (\mathbf{X} - \mathbf{X}_k)^T \nabla f(\mathbf{X}_k) + \frac{1}{2!} (\mathbf{X} - \mathbf{X}_k)^T \mathbf{H}(\mathbf{X}_k) (\mathbf{X} - \mathbf{X}_k) + o((\mathbf{X} - \mathbf{X}_k)^T (\mathbf{X} - \mathbf{X}_k)) \quad (11)$$

wherein the independent variable is

$$\mathbf{X} = (x_1, x_2, \dots, x_n)^T \quad (12)$$

$$\mathbf{X}_k = (x_1^{(k)}, x_2^{(k)}, \dots, x_n^{(k)})^T \quad (13)$$

$\nabla f(\mathbf{X}_k)$ is the function $f(\mathbf{X})$ at point \mathbf{X}_k gradient on the point where

$$\nabla f(\mathbf{X}) = \left(\frac{\partial f(\mathbf{X})}{\partial x_1}, \frac{\partial f(\mathbf{X})}{\partial x_2}, \dots, \frac{\partial f(\mathbf{X})}{\partial x_n} \right) \quad (14)$$

\mathbf{H} for the Hessian matrix:

$$\mathbf{H} = \begin{pmatrix} \frac{\partial^2 f(\mathbf{X})}{\partial x_1^2} & \frac{\partial^2 f(\mathbf{X})}{\partial x_1 \partial x_2} & \dots & \frac{\partial^2 f(\mathbf{X})}{\partial x_1 \partial x_n} \\ \frac{\partial^2 f(\mathbf{X})}{\partial x_2 \partial x_1} & \frac{\partial^2 f(\mathbf{X})}{\partial x_2^2} & \dots & \frac{\partial^2 f(\mathbf{X})}{\partial x_2 \partial x_n} \\ \vdots & \vdots & \ddots & \vdots \\ \frac{\partial^2 f(\mathbf{X})}{\partial x_n \partial x_1} & \frac{\partial^2 f(\mathbf{X})}{\partial x_n \partial x_2} & \dots & \frac{\partial^2 f(\mathbf{X})}{\partial x_n^2} \end{pmatrix} \quad (15)$$

Due to the availability of the second-order multivariate Taylor formula, employing the least-squares method for quadratic regression in multivariate functions is viable. That is when the argument is

$$\mathbf{X} = (x_1, x_2, \dots, x_n)^T \quad (16)$$

There are

$$\mathbf{X}^* = (x_1^2, x_2^2, \dots, x_n^2, x_1 x_2, x_1 x_3, \dots, x_i x_j, \dots, x_{n-1} x_n, x_1, x_2, \dots, x_n, 1)^T \quad (17)$$

Here assignment:

$$\mathbf{X}^* = \mathbf{Z} = (z_1, z_2, \dots, z_m)^T \quad (18)$$

where $m = n^2 + n + 1$. Then, the original problem of fitting \mathbf{X} was transformed into the issue of fitting \mathbf{Z} .

Based on the previous discussion, 43 experiments were designed to prepare Mg–Al LDH films under different reaction conditions. As shown in Table 1, the corresponding polarization curves were tested (detailed information is shown in Figure S1 and Table S1), and utilizing these data, a regression model of corrosion current density (I_{corr}) in relation to the concentration of reaction temperature T (x), pH (y), and reaction time t (z) was established. Set up:

$$x = T$$

$$y = \text{pH}$$

$$z = t$$

The data are processed logarithmically and then fitted linearly using the least-squares method in the following form:

$$\ln I_{\text{corr}} = \beta_0 + \beta_1 x^2 + \beta_2 y^2 + \beta_3 z^2 + \beta_4 xy + \beta_5 xz + \beta_6 yz + \beta_7 x + \beta_8 y + \beta_9 z$$

Get the results:

$$\begin{pmatrix} \beta_0 \\ \beta_1 \\ \beta_2 \\ \beta_3 \\ \beta_4 \\ \beta_5 \\ \beta_6 \\ \beta_7 \\ \beta_8 \\ \beta_9 \end{pmatrix} = \begin{pmatrix} 7.385714 \\ 0.00069 \\ 0.173217 \\ 0.014209 \\ -0.01154 \\ -0.00326 \\ 0.017771 \\ 0.000669 \\ -3.07236 \\ -0.29223 \end{pmatrix}$$

$$R^2 = 0.848$$

$$p < 0.05$$

where R^2 represents the goodness of fit, a higher R^2 value, closer to 1, indicates a better fit of the regression equation to the test values. The P value represents the significance test of the equation.³² With a goodness of fit reaching 0.848 and a P value less than 0.05, indicating a confidence level of 95%, these conditions suggest that the regression equation for each index fits well with the experimental results at the test points studied in this paper. It demonstrates a high degree of fit with the experimental results throughout the entire research scope. Residual analysis was performed to further analyze the relevant results. The residual data are shown in Table S2, and Figure 1 is plotted based on it.

Assuming the confidence level of the residual value is within the 95% confidence interval. In this case, the difference between the fitting and experimental results is insignificant, and the confidence level of the fitting result can reach 95%. In Figure 1, output by the rcoplot function built in MATLAB, each data point's residual is depicted with a circle. The straight line in the middle is 0, and the residual above the 0 lines is positive, whereas the residual below the 0 lines is negative. Each dot is in a confidence interval, which is shown as a line segment with this data point as the midpoint, that is, vertical lines in the figure. If line 0 crosses the line segment where the data point is located, it implies that 0 is within the confidence interval and the difference between the experimental data and itself is 0. Hence, the experimental data are within the confidence interval, and the fitting result is relatively close to the practical result. The confidence value represents the experimental value of the residual error within the confidence interval, while the nonconformity value represents the experimental value of the residual error outside the confidence interval. Following the residual analysis of 43 groups, it can be concluded that only two line segments and Line 0 do not share a common point. It means that among all the data, 43 data points have residuals that satisfy a 95% confidence level, achieving an accuracy rate of 95.35%. However, due to potential errors in data analysis, verification through experiments is still necessary.

The fmincon function built in MATLAB determined that the optimal corrosion-resistant film will be achieved when the parameters are set to $T = 135$ °C, pH 12.0, and $t = 15$ h. Then, the sample was prepared according to these experimental

Table 1. Design of Experiment and Experimental Results

sample numbers	temperature (T , °C)	pH	time (t , h)	I_{corr} (A/cm^2)
1	60	9	3	2.54×10^{-05}
2	60	12	9	1.30×10^{-05}
3	60	13	9	1.51×10^{-05}
4	60	12	15	9.46×10^{-06}
5	90	12	9	6.34×10^{-06}
6	120	8	9	1.44×10^{-05}
7	120	9	9	8.19×10^{-06}
8	120	10	9	9.85×10^{-07}
9	120	11	9	8.77×10^{-07}
10	120	12	9	3.57×10^{-07}
11	120	13	9	5.54×10^{-07}
12	120	12	3	7.22×10^{-06}
13	120	12	6	1.06×10^{-06}
14	50	12	10	1.32×10^{-05}
15	110	12	6	1.25×10^{-06}
16	110	9	10	7.01×10^{-06}
17	120	12	2	1.66×10^{-05}
18	130	12	10	4.91×10^{-07}
19	120	12	5	2.47×10^{-06}
20	145	12	13	9.41×10^{-07}
21	120	12	12	2.39×10^{-07}
22	120	12	15	1.34×10^{-07}
23	120	13	15	8.70×10^{-07}
24	150	13	3	9.87×10^{-06}
25	150	12	9	8.56×10^{-07}
26	150	9	15	4.07×10^{-06}
27	110	13	10	4.49×10^{-07}
28	110	11	10	5.26×10^{-07}
29	110	12	10	3.47×10^{-07}
30	70	12	10	7.28×10^{-06}
31	110	12	4	6.88×10^{-07}
32	130	13	4	1.69×10^{-06}
33	50	12	8	1.40×10^{-05}
34	130	9	8	6.32×10^{-06}
35	50	9	4	1.57×10^{-05}
36	120	12	4	3.67×10^{-06}
37	70	12	12	1.25×10^{-05}
38	120	12	8	6.77×10^{-07}
39	145	12	15	5.04×10^{-07}
40	120	12	18	2.06×10^{-07}
41	120	12	21	2.42×10^{-07}
42	130	13	18	3.15×10^{-07}
43	140	10	18	8.12×10^{-07}

conditions, and the corrosion resistance was tested. The experimental results showed that corrosion current density $I_{\text{corr}} = 1.07 \times 10^{-7} \text{ A}/\text{cm}^2$. It is found that the overall variance follows a normal distribution with an expectation of 1×10^{-15} and a conflict of 0.6021, resulting in an absolute residual value of 0.8806. If $R \sim N(0, 0.8806)$, then $P(R \leq 0.8806) = 0.9282$. Therefore, the experimental value is within a 95% confidence interval of the predicted value, where N is the normal distribution, R is the probability, and P is the residual. The above result indicates that the experimental results agree with the model, so the model can effectively predict the optimal process parameters.

4. CHARACTERIZATION OF MG–AL LDH FILMS

4.1. Morphology, Structure, and Composition of Mg–Al LDH Films. The Mg–Al LDH films were hydrothermally

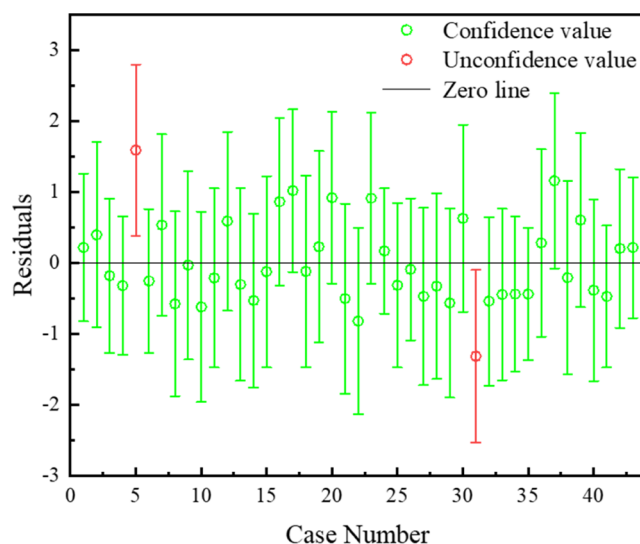


Figure 1. Residual figure of experimental values.

synthesized on the surface of magnesium alloy at $T = 135 \text{ }^\circ\text{C}$, $\text{pH} = 12.0$, and $t = 15 \text{ h}$ according to the results derived in this paper. SEM and EDS spectra of the obtained Mg–Al LDH films and their immersion in 3.5 wt % NaCl solution for 180 h are shown in Figure 2. From Figure 2a1, it can be found that the outer layer of the Mg–Al LDH film prepared under this condition presents a typical interlaced nanosheet structure of LDH, and the surface layer of the nanosheet has a uniform distribution.³² The thickness of the LDH film is about $5.3 \text{ }\mu\text{m}$ based on its cross section (Figure 2a2). In addition, the inner layer of the LDH film is relatively dense and uniformly attached to the surface of the magnesium alloy, it is consistent with the cross-sectional results of Kosari et al.³³ They used TEM analysis on the LDH film and found the presence of a dense inner layer in the LDH film, which could effectively prevent chloride ion penetration and subsequent attack of the magnesium alloy substrate. The EDS spectra (Figure 2a3) showed that the film mainly comprises C, N, O, Mg, and Al elements after the Mg–Al LDH film immersion in 3.5 wt % NaCl solution for 180 h, many precipitates covered on the LDH film (Figure 2b1), which indicates that the outer layer of LDH film corroded locally, and clusters are formed to cover the film's surface. These clusters can physically block oxygen diffusion, thus inhibiting the reduction reaction in the corrosion process and leading to a delay in the further corrosion of these initial corroded areas. The inner layer is rough and porous, caused by the film's slow dissolution due to Cl^- corrosion. Nevertheless, the film is still completely covered on the magnesium alloy surface, which can prevent the penetration of Cl^- to the matrix. From the EDS results, it can be found that the content of Mg and Al elements in the sample after immersion has decreased compared with that before immersion, which indicates the dissolution of the film. At the same time, Cl^- is detected in the film after immersion due to the LDH corrosion resistance mechanism. The corrosion protection mechanism of LDH is not a simple physical barrier effect in addition to its ion exchangeability to adsorb the anions in the corrosive medium while in between the layers, thus achieving a double protection effect on the substrate.²⁰

The XRD patterns of the AZ91D magnesium alloy and Mg–Al LDH film are shown in Figure 3a. It can be seen that the diffraction peak intensity of the magnesium alloy substrate is very high for the Mg–Al LDH sample. In contrast, the peak

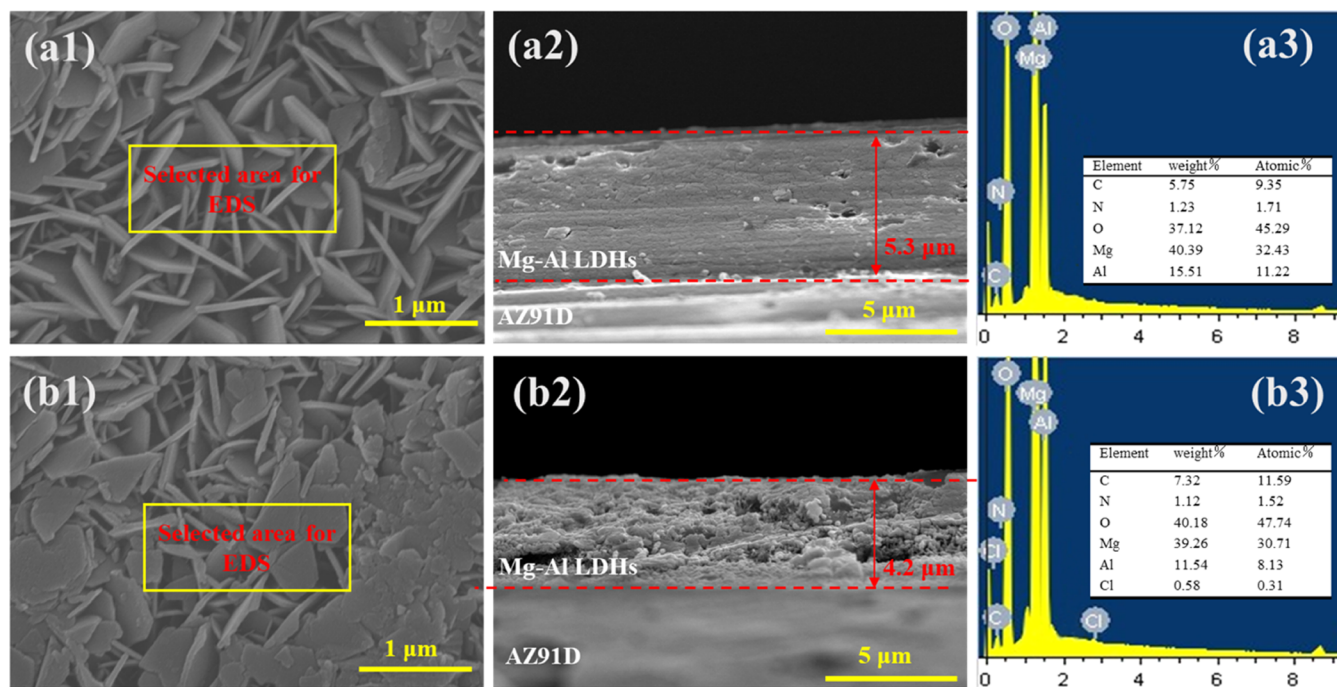


Figure 2. Surface (a1, b1), cross section (a2, b2) micrograph, and energy spectrum (a3, b3) of Mg–Al LDH (a) and Mg–Al LDH immersed in 3.5 wt % NaCl solution for 180 h (b).

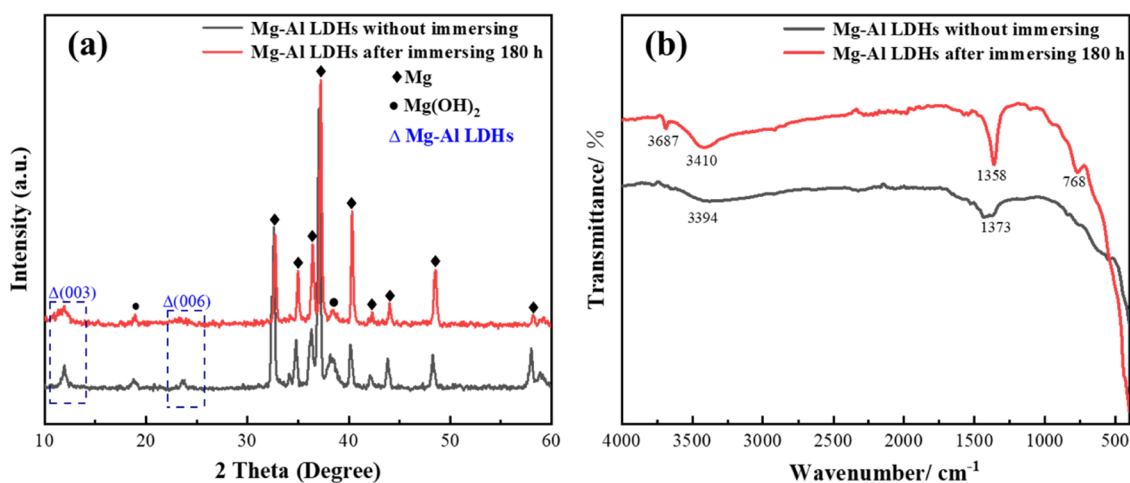
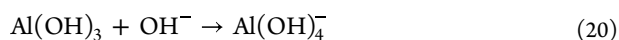
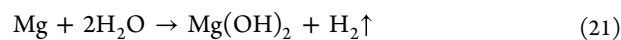


Figure 3. (a) XRD patterns of the AZ91D magnesium alloy and Mg–Al LDH film and (b) FT-IR spectra of the Mg–Al LDH film before and after immersion.

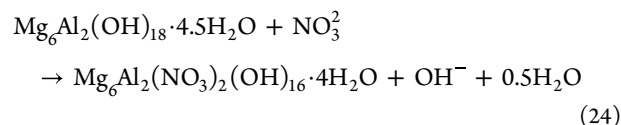
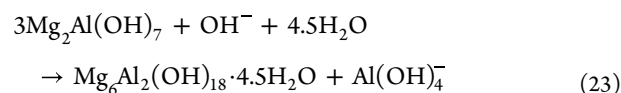
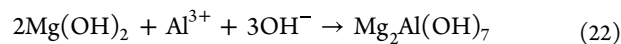
intensity of the Mg–Al LDH is weaker because the penetration depth of the X-rays is much greater than that of the LDH film layer. At the same time, the characteristic diffraction peaks with 2θ values positioned at 11.66° and 20.56° correspond to (003) and (006) reflections of LDH (JCPDS # 41-1482).²⁴ This result is similar to the results in the literature.^{16,34} In the synthetic process, LDH films undergo hydrothermal reactions, and the detailed chemical reactions on the surface of Mg are as follows: First, Al^{3+} reacts with OH^- in an alkaline solution:



Magnesium alloy conducts slight anodic dissolution and generates $\text{Mg}(\text{OH})_2$ in alkaline environments:



Therefore, the formation mechanism of LDH results from partial Mg^{2+} ions in $\text{Mg}(\text{OH})_2$ replaced by Al^{3+} ions in the presence of high-temperature and high-pressure environments. The chemical reactions are as follows:³⁵



Note that the characteristic diffraction peaks of LDH corresponding to (003) and (006) reflections were still observed after the samples were immersed in 3.5 wt % NaCl solution for 180 h, except that the (006) characteristic diffraction peaks' relative intensity decreased and showed broadening phenomena. To further explore the grain size change of LDH, the Scherrer Equation³⁵ is used to calculate the grain size of each sample:

$$D = \frac{K\gamma}{B \cos \theta} \quad (25)$$

where D is the average thickness of the grain perpendicular to the crystal plane, K is the Scherrer constant being 0.89, B is the half peak width of the measured sample diffraction peak, θ is the corner of Prague, and γ is the X-ray wavelength with 0.154056 nm. It is calculated that the grain size of the LDH film before immersion is 19.97 nm, while it drops to 5.08 nm after immersion. The decrease in grain size may be due to the grain refinement phenomenon caused by corrosion and ion exchange between the LDH film and external anions.^{20,35} According to relevant literature, grain refinement can increase the free energy of the film, thereby decreasing the potential of the battery electrode and making the film more susceptible to corrosion from a thermodynamic perspective. However, the film becomes denser after grain refinement, which protects the matrix from further deterioration from local disintegration.^{34–36} The characteristic peaks of the Mg–Al LDH film on the substrate surface remained after the 180 h of immersion test. Therefore, the SEM and XRD tests proved that the Mg–Al LDH film layer prepared on the Mg alloy surface under the optimal conditions of the hydrothermal method using the mathematical model was deduced to have better protection corrosion-inhibiting stability.

Figure 3b shows the FT-IR spectra of the Mg–Al LDH film before and after immersion, and it can be found that the characteristic peaks of the two are similar. The absorption peak at 3410 cm^{-1} is the H–O–H stretching vibration peak. The typical peak at 1373 cm^{-1} may be ascribed to the stretching vibration of NO_3^- in LDH layer spacing and the asymmetric stretching vibration of CO_3^{2-} .^{37,38} The NO_3^- in the film mainly comes from Al (NO_3)₃. The anions intercalated in the LDH film prepared in this scheme are mostly NO_3^- , while CO_3^{2-} comes from trace CO_2 in an aqueous solution. In addition, several absorption peaks at 600–900 cm^{-1} may be lattice vibration peaks from M–OH and M–O (M = Mg, Al).³⁹ The only difference is the occurrence of an absorption peak at 3687 cm^{-1} for the Mg–Al LDH film after 180 h immersion, which is attributed to the formation of Mg (OH)₂ precipitation after corrosion.²⁰

4.2. Corrosion Resistance of Mg–Al LDH Films. Figure 4 depicts the test results of the potential dynamic polarization curves of blank magnesium alloy, and it is covered with the Mg–Al LDH film before and after 180 h immersion in 3.5 wt % NaCl solution. It is evident that after the LDH film is prepared on the magnesium alloy surface by the hydrothermal method, the current density of its anode and cathode branches decreases, which indicates that the coating inhibits the dissolution reaction of anode magnesium ($\text{Mg} - 2\text{e}^- \rightarrow \text{Mg}^{2+}$) and cathodic oxygen reduction ($\text{O}_2 + 2\text{H}_2\text{O} + 4\text{e}^- \rightarrow 4\text{OH}^-$). Corrosion potential (E_{corr}), corrosion current density (I_{corr}), and anodic and cathodic slope (b_a and b_c) are listed in Table 2. From Table 2, it can be seen that the E_{corr} values before and after 180 h immersion in 3.5 wt % NaCl solution of magnesium alloy covered with the Mg–Al LDH film and blank magnesium alloy were -1.354 to -1.441

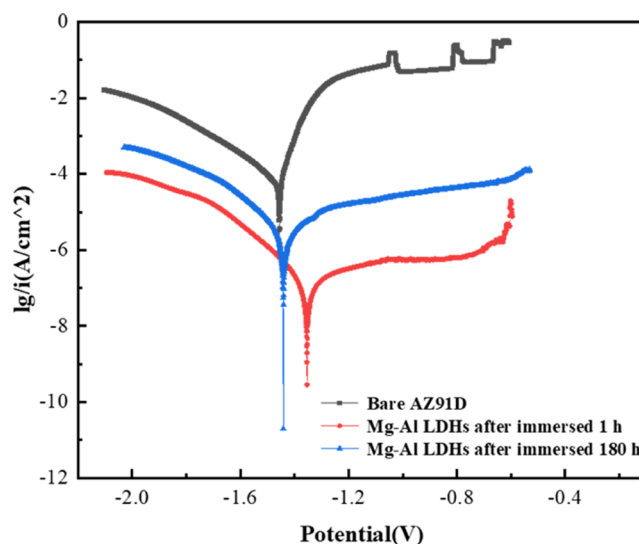


Figure 4. Polarization curves of AZ91D covered with Mg–Al LDH films before and after immersion in 3.5 wt % NaCl solution for 180 h and bare AZ91D.

and -1.516 V vs SCE, respectively. Also, the corrosion current density of the sample after 180 h immersion (1.61×10^{-6} A/ cm^2) was higher than that for 1 h immersion (1.07×10^{-7} A/ cm^2). Although the corrosion current decreased significantly, it remained 2 orders of magnitude higher than the untreated blank magnesium alloy, indicating that the Mg–Al LDH film possessed good protective durability. To further investigate the internal changes of the film layer, the porosity of the film layer can be estimated using the following relational equation:^{40,41}

$$R_p = \frac{b_a \times b_c}{2.303 \times I_{\text{corr}} \times (b_a + b_c)} \quad (26)$$

$$P = \frac{R_{ps}}{R_{pc}} \times 10^{-[|\Delta E_{\text{corr}}|/b_a]} \quad (27)$$

In the equation, b_a and b_c denote the anodic and cathodic Tafel slopes, respectively. I_{corr} is the corrosion current density (A/ cm^2). P represents the total porosity of the film, and ΔE_{corr} represents the difference between the open circuit potential of the magnesium alloy substrate and the LDH film. R_p represents the polarization resistance, R_{ps} represents the matrix polarization resistance, and R_{pc} represents the polarization resistance of the LDH film. The calculation shows that the porosity of Mg–Al LDH film increased from 0.036 to 0.538% after immersion in 3.5 wt % NaCl, which is an order of magnitude increase, but still maintains a low porosity, so the overall protection durability of the film is good.

EIS is another powerful technique to evaluate corrosion protection performance. The protective durability of the film was analyzed by comparing the electrochemical parameters of the Mg alloy covered with Mg–Al LDH film before and after 180 h immersion in 3.5 wt % NaCl solution (Figure 5). The Nyquist plots of EIS in Figure 5a,b are imperfect semicircles, meaning the test system is not an ideal capacitor. It can be found from Figure 5a that for the sample after immersion in 3.5 wt % NaCl solution for 180 h, the radius of the capacitive reactance arc decreases significantly. The appearance of an inductive reactance arc in the low-frequency region is mainly caused by the

Table 2. Tafel Parameters of AZ91D and AZ91D Covered with Mg–Al LDH Films Before and After Immersion in 3.5 wt % NaCl Solution for 180 h

sample	E_{corr} (V vs SCE)	I_{corr} (A/cm ²)	b_c (mV·dec ⁻¹)	b_a (mV·dec ⁻¹)	R_p (Ω·cm ²)	porosity (%)
AZ91D Mg alloy	-1.516	1.940×10^{-4}	149.70	58.83	94.53	
Mg–Al LDH (immersed 1 h)	-1.354	1.070×10^{-7}	99.68	188.04	264 368.99	0.036
Mg–Al LDH (immersed 180 h)	-1.441	1.611×10^{-6}	122.55	138.97	17 563.44	0.538

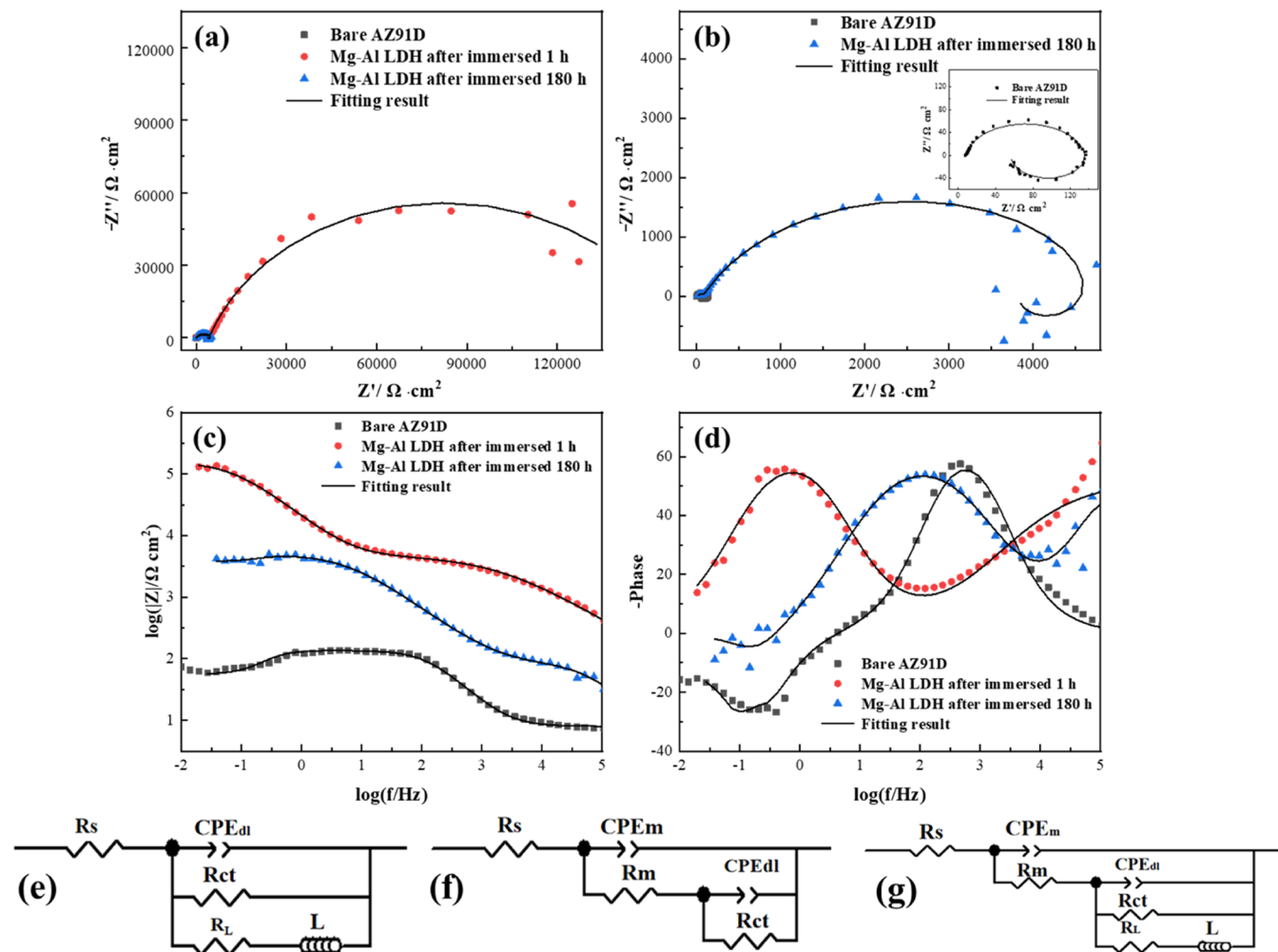


Figure 5. Nyquist plots (a, b), Bode plots (c, d), and the equivalent circuit diagrams (e–g) of AZ91D covered with Mg–Al LDH films before and after immersion in 3.5 wt % NaCl solution for 180 h and AZ91D.

anions' characteristic adsorption of the film.⁴² The adsorption is attributed to the anion-exchange capacity of the Mg–Al LDH films, releasing NO_3^- between layers, and then Cl^- in the solution is exchanged to the LDH layer. However, the capacitive arc radius of the sample immersed for 180 h is much larger than the blank magnesium alloy. The larger capacitive arc radius indicates that the magnesium alloy's overall corrosion resistance covered with Mg–Al LDH film is still better than the blank magnesium alloy even after 180 h immersion. This result further indicates that the Mg–Al LDH film obtained under this condition has good corrosion durability. The capacitance circuit in the high-frequency and intermediate-frequency regions of Bode plots (Figure 5c,d) mainly characterizes the electrochemical process of the outer layer. The electrochemical behavior in the low-frequency region is primarily associated with the interface between the film and the substrate. Based on the analysis of the characteristics of Nyquist plots (Figure 5a,b)

and Bode plots (Figure 5c,d) obtained from the electrochemical test, the electrochemical equivalent circuit in Figure 5e–g can be used to fit the EIS plots (Figure 5b–d) of the AZ91D substrate and magnesium alloy covered with the Mg–Al LDH film before and after immersion. The relevant results are given in Table 3.

The EIS diagrams of AZ91D substrates and magnesium alloys covered with Mg–Al LDH film layers before and after immersion were fitted by the time constant method proposed by Wit,⁴³ using the equivalent circuit plots of Figure 5e–g. Two equivalent circuit diagrams (Figure 5e,f) are used to simulate the EIS results and quantitatively compare the corrosion resistances of different films. The corresponding electrochemical parameters obtained by Z-view fitting are given in Table 3. R_s is the solution resistance, R_l is the film resistance, R_{ct} is the electrochemical reaction resistance, and R_p is the total corrosion resistance of LDH. Generally speaking, the greater the R_p value, the better the corrosion resistance of the reaction film. Notably,

Table 3. EIS Fitting Results of AZ91D and AZ91D Covered with Mg–Al LDH Films Before and After Immersion in 3.5 wt % NaCl Solution for 180 h

sample	blank Mg alloy	Mg–Al LDH (immersed for 1 h)	Mg–Al LDH (immersed for 180 h)
R_s ($\Omega\text{-cm}^2$)	7.957	9.510	10.08
CPE_m (F/cm^2)		9.45×10^{-7}	1.34×10^{-5}
R_m ($\Omega\text{-cm}^2$)		4.71×10^3	2.73×10^3
n_1		0.58	0.66
CPE_{dl} (F/cm^2)	1.95×10^{-5}	1.08×10^{-5}	5.03×10^{-5}
R_{ct} ($\Omega\text{-cm}^2$)	1.29×10^2	1.58×10^5	5.81×10^3
n_2	0.91	0.80	0.79
R_L ($\Omega\text{-cm}^2$)	77.6		3.14×10^3
L_L (H/cm^2)	96.6		6.23×10^3
R_{total} ($\Omega\text{-cm}^2$)	2.06×10^2	1.62×10^5	1.68×10^4

the capacitance loops in the Nyquist diagram are not perfect semicircles, and their center is lower than the X-axis. A constant phase element (CPE) is used to replace the ideal capacitance Q , and n ($0 < n < 1$) is introduced to calibrate the actual capacitance. The factor n represents the coefficient of deviation between the capacitance obtained from the system and the ideal capacitance C . The factor n also represents the frequency power of CPE; $n = 1$ means CPE is a perfect capacitor (C). Nonideal capacitive loops can result from surface roughness and nonuniformity.⁴⁴ The impedance of CPE can be calculated using the following equation.⁴⁵

$$Z_{CPE} = [Q(j\omega)^n]^{-1} \quad (28)$$

Q is the modulus, ω is the angular frequency, and n is the phase shift reflecting the surface inhomogeneity.

CPE_1 is the film capacitance, CPE_{dl} is the double-layer capacitance, and L is an inductive element.

R_{total} is defined as the sum of the coating resistance, charge transfer resistance, and inductance resistance and provides an evaluation of protection efficiency (PE). In general, the larger the R_{total} , the higher the PE of the LDH film.⁴⁶

$$R_{total} = R_m + R_{ct} + R_L \quad (29)$$

It can be seen from Table 3 that the magnesium alloy covered with Mg–Al LDH film after immersion for 180 h, the R_{ct} decreased from $1.58 \times 10^5 \Omega/\text{cm}^2$ to $5.81 \times 10^3 \Omega/\text{cm}^2$, reduced by about 2 orders of magnitude. In contrast, the total corrosion resistance R_{total} decreased by 1 order of magnitude from $1.62 \times 10^5 \Omega/\text{cm}^2$ drops to $1.68 \times 10^4 \Omega/\text{cm}^2$. However, the R_{total} of the sample is still 2 orders of magnitude higher than that of the blank magnesium alloy. After 180 h immersion, the total capacitance ($CPE_m + CPE_{dl}$) of LDH increased slightly (from about $1.117 \times 10^{-5} F/\text{cm}^2$ increased to $6.37 \times 10^{-5} F/\text{cm}^2$). Combined with the changes in the film surface structure, film thickness, and element types in SEM (Figure 2a1,b1), it can be deduced that the increase in capacitance may be mainly ascribed to the presence of Cl^- . The Cl^- deterioration changes the film's interlayer spacing. Increasing the interlamellar spacing will ultimately lead to a change in the total area of the LDH film.⁴⁷ The difference in the total capacitance of the film before and after immersion is slight, indicating that the film's overall structure changes little. In summary, the corrosion resistance of

the Mg–Al LDH film decreased after 180 h immersion; nevertheless, the Mg–Al LDH film still gave good protection to the Mg alloy.

5. CONCLUSIONS

Based on the multivariate polynomial regression fitting method, this study derived a synergistic equation of reaction temperature, pH, and reaction time for the corrosion resistance of Mg–Al LDH films on magnesium alloy surfaces prepared by the hydrothermal method. The equation was based on the reaction temperature, pH, and reaction duration time. Then, the optimal preparation conditions for the corrosion resistance of the thin film were determined based on the derived equation. Finally, the structure, composition, corrosion resistance, and durability of the LDH film prepared under optimal preparation conditions were studied. The main conclusions are summarized as follows:

- (1) A synergistic relationship equation was fitted for the effects of reaction temperature, pH, and the reaction duration time on the corrosion resistance of LDH films. The confidence of multivariate polynomial regression equations can reach 95%, and the regression equation has high accuracy in predicting the corrosion current density of samples prepared by the hydrothermal method. The fitting results showed that the Mg–Al LDH film had the best corrosion resistance when prepared at $T = 135 \text{ }^\circ\text{C}$, $pH = 12.0$, and $t = 15 \text{ h}$.
- (2) The microscopic images showed that the Mg–Al LDH film prepared under the above conditions remained intact on the surface of the magnesium alloy after 180 h immersion in 3.5 wt % NaCl aqueous solution. XRD showed that the characteristic peaks of LDH were still present with a finer grain. The electrochemical test found that the corrosion current density of the sample increased from 1.07×10^{-7} to $1.61 \times 10^{-6} \text{ A}/\text{cm}^2$, and the total corrosion resistance decreased from 1.62×10^5 to $1.68 \times 10^4 \Omega\text{-cm}^2$ after immersion in 3.5 wt % NaCl solution for 180 h. However, the corrosion resistance remained more than 2 orders of magnitude higher than that of the blank Mg alloy in 3.5 wt % NaCl solution after 180 h immersion indicates that the Mg–Al LDH film, prepared under the optimal conditions derived from the multivariate linear equation, has good protective durability for magnesium alloys.

ASSOCIATED CONTENT

Supporting Information

The Supporting Information is available free of charge at <https://pubs.acs.org/doi/10.1021/acsomega.3c10297>.

Polarization curve corresponding to samples numbered 1–43; polarization parameters corresponding to potentiodynamic polarization curve of samples 1–43; residual value and residual interval of samples numbered 1–43 (PDF)

AUTHOR INFORMATION

Corresponding Authors

Xiaoqing Du – School of Materials Science and Hydrogen Energy, Foshan University, Foshan 528011, China; orcid.org/0000-0002-7869-575X; Email: amyzju88@163.com

Dongchu Chen — School of Materials Science and Hydrogen Energy, Foshan University, Foshan 528011, China; Email: chendc@fosu.edu.cn

Authors

Chengfeng Wang — School of Materials Science and Hydrogen Energy, Foshan University, Foshan 528011, China; School of Materials Science and Engineering, Nanchang Hangkong University, Nanchang 330063, China

Bofan Liu — School of Science, Beijing University of Posts and Telecommunications, Beijing 100876, China; Software Development Centre of Bank of Beijing, Beijing 100013, China

Pengxu Wei — School of Materials Science and Hydrogen Energy, Foshan University, Foshan 528011, China

Kepei Xie — School of Materials Science and Hydrogen Energy, Foshan University, Foshan 528011, China

Yu Chen — School of Materials Science and Hydrogen Energy, Foshan University, Foshan 528011, China

Meifeng Wang — School of Materials Science and Engineering, Nanchang Hangkong University, Nanchang 330063, China

Complete contact information is available at:

<https://pubs.acs.org/10.1021/acsomega.3c10297>

Notes

The authors declare no competing financial interest.

ACKNOWLEDGMENTS

This research was funded by the Key-Area Research and Development Program of Guangdong Province (2020B010186001), the National Natural Science Foundation of China (52101079), Guangdong Basic and Applied Basic Research Foundation (2020B1515120093), and Science and Technology Project of Guangdong Province (2020B121202002).

REFERENCES

- (1) Song, Y.; Shan, D.; Han, E. Pitting corrosion of a Rare Earth Mg alloy GW93. *J. Mater. Sci. Technol.* **2017**, *33*, 954–960.
- (2) Chaudry, U. M.; Farooq, A.; Tayyab, K.; et al. Corrosion behavior of AZ31 magnesium alloy with calcium addition. *Corros. Sci.* **2022**, *199*, No. 110205.
- (3) Mardali, M.; Hamidreza, S.; Fathallah, K.; et al. Microstructure and Corrosion Characterization of a MgO/Hydroxyapatite Bilayer Coating by Plasma Electrolytic Oxidation Coupled with Flame Spraying on a Mg Alloy. *ACS Omega* **2020**, *5* (38), 24186–24194.
- (4) Wu, W.; Xiaoming, Y.; Yan, Z.; et al. Characterization and Biocompatibility of Insoluble Corrosion Products of AZ91 Mg Alloys. *ACS Omega* **2019**, *4* (12), 15139–15148.
- (5) Wang, X.; Wang, W.; Chen, W.; Chen, D. Effect of Al addition and heat treatment on the microstructures and corrosion resistance of Mg-Cu alloys. *J. Mater. Sci. Technol.* **2022**, *98* (30), 219–232.
- (6) Prabhu, D. B.; Gopalakrishnan, P.; Ravi, K. Morphological studies on the development of chemical conversion coating on the surface of Mg-4Zn alloy and its corrosion and biomineralization behavior in simulated body fluid. *J. Alloys Compd.* **2020**, *812*, 152146 DOI: [10.1016/j.jallcom.2019.152146](https://doi.org/10.1016/j.jallcom.2019.152146).
- (7) Geng, Z.; Li, X.; Zhang, Y.; et al. Corrosion resistance and degradation behavior of anodized Mg-Gd alloys: A comparative study. *Surf. Coat. Technol.* **2021**, *412* (11), No. 127042.
- (8) Singh, C.; Singh, C.; Tiwari, S. K.; et al. Development of corrosion-resistant electroplating on AZ91 Mg alloy by employing air and water-stable eutectic based ionic liquid bath. *Surf. Coat. Technol.* **2021**, *428*, No. 127881.
- (9) Wang, Z.-C.; Yu, L.; Qi, Z. B.; Song, G. L. Electroless Nickel-Boron Plating to Improve the Corrosion Resistance of Magnesium (Mg) Alloys. In *Corrosion Prevention of Magnesium Alloys*; Woodhead Publishing, 2013; pp 370–392.
- (10) Kumaradhas, P.; Sivapragash, M. Comparison of corrosion behavior of heat treated, ZrO₂ and ZrN PVD coated AZ91D Mg alloy. *Mater. Today: Proc.* **2022**, *56*, 527–532.
- (11) Selegred, L.; Poot, T.; Eriksson, P.; et al. In-Situ Growth of Cerium Nanoparticles for Chrome-Free, Corrosion Resistant Anodic Coatings. *Surf. Coat. Technol.* **2021**, *410*, No. 126958.
- (12) Cheng, S.; Lan, L.; Li, M.; et al. Pure Mg–Al Layered Double Hydroxide Film on Magnesium Alloys for Orthopedic Applications. *ACS Omega* **2021**, *6* (38), 24575–24584.
- (13) Liu, L.; Dong, S.; Wang, F.; et al. Fabrication of uniform and anti-corrosion layered double hydroxides film on Mg-Gd-Y-Zn-Zr alloy through solution pH tailoring. *Electrochim. Acta* **2022**, *411* (10), No. 140057.
- (14) Cao, Y.; Zheng, D.; Zhang, F.; et al. Layered double hydroxide (LDH) for multi-functionalized corrosion protection of metals: A review. *J. Mater. Sci. Technol.* **2022**, *102*, 232–263.
- (15) Yan, H.; Lu, J.; Wei, M.; et al. Theoretical study of the hexahydrated metal cations for the understanding of their template effects in the construction of layered double hydroxides. *J. Mol. Struct.: THEOCHEM* **2008**, *866* (1), 34–45.
- (16) Zhou, M.; Yan, L.; Ling, H.; et al. Design and fabrication of enhanced corrosion resistance Zn-Al layered double hydroxides films based anion-exchange mechanism on magnesium alloys. *Appl. Surf. Sci.* **2017**, *404*, 246–253.
- (17) Gu, Z.; Huang, Y.; Wang, Y.; et al. An aluminum silicate modified Ni-Al LDH film to improve the corrosion resistance of AZ31 Mg alloy. *Mater. Lett.* **2019**, *252*, 304–307.
- (18) Tan, J. K. E.; Balan, P.; Birbilis, N. Advances in LDH coatings on Mg alloys for biomedical applications: A corrosion perspective. *Appl. Clay Sci.* **2020**, *202* (4), No. 105948, DOI: [10.1016/j.clay.2020.105948](https://doi.org/10.1016/j.clay.2020.105948).
- (19) Hou, L.; Li, Y.; Sun, J.; et al. Enhancement corrosion resistance of Mg-Al layered double hydroxides films by anion-exchange mechanism on magnesium alloys. *Appl. Surf. Sci.* **2019**, *487*, 101–108.
- (20) Kamiyama, N.; Panomsuwan, G.; Yamamoto, E.; et al. Effect of treatment time in the Mg(OH)₂/Mg-Al LDH composite film formed on Mg alloy AZ31 by steam coating on the corrosion resistance. *Surf. Coat. Technol.* **2016**, *286* (7), 172–177.
- (21) Chen, J.; Fang, L.; Wu, F.; et al. Corrosion resistance of a self-healing rose-like MgAl-LDH coating intercalated with aspartic acid on AZ31 Mg alloy. *Prog. Org. Coat.* **2019**, *136* (12), No. 105234.
- (22) Wang, X.; Xian, W.; Li, L.; Xie, Z. Duplex coating combining layered double hydroxide and 8-quinolinol layers on Mg alloy for corrosion protection. *Electrochim. Acta* **2018**, *283*, 1845–1857.
- (23) Chen, J.; Song, Y.; Shan, D.; Han, E. H. In Situ Growth Process of Mg-Al Hydroxide Conversion Film on AZ31 Mg Alloy. *J. Mater. Sci. Technol.* **2015**, *31* (31), 384–390.
- (24) Lin, J.; Uan, J. Formation of Mg-Al-hydroxide conversion coating on Mg alloy in aqueous HCO₃⁻/CO₃²⁻ and corresponding protection against corrosion by the coating. *Corros. Sci.* **2009**, *51* (5), 1181–1188.
- (25) Mitchell, S.; Biswick, T.; Jones, W.; et al. A synchrotron radiation study of the hydrothermal synthesis of layered double hydroxides from MgO and Al₂O₃ slurries. *Green Chem.* **2007**, *9* (4), 373–378.
- (26) Li, X.; Zhang, D.; Liu, Z.; et al. Share corrosion data. *Nature* **2015**, *527* (7579), 441–442.
- (27) Pei, Z.; Zhang, D.; Zhi, Y.; et al. Towards understanding and prediction of atmospheric corrosion of a Fe/Cu corrosion sensor via machine learning. *Corros. Sci.* **2020**, *170*, No. 108697, DOI: [10.1016/j.corsci.2020.108697](https://doi.org/10.1016/j.corsci.2020.108697).
- (28) Haynie, F.; Upham, J. Effects of atmospheric pollutants on corrosion behavior of steels. *Mater. Prot.* **1971**, *10* (11), 18–21.
- (29) Zor, S.; Erten, U.; Bing, D. Investigation of the effect of physical conditions of a coating bath on the corrosion behavior of zinc coating using response surface methodology. *Prot. Met. Phys. Chem. Surf.* **2015**, *51* (2), 304–309.

- (30) Wang, Z.; Ma, Y.; Liang, Z.; et al. Effect of electrolytes and their interaction on the corrosion resistance of micro-arc oxidation coating of A356 Al alloy. *Chin. J. Nonferrous Met.* **2023**, *33* (02), 549–564.
- (31) Apostol, T. *Mathematical Analysis*; Addison-Wesley, 1973.
- (32) Breig, S. J. M.; Luti, K. Response surface methodology: A review on its applications and challenges in microbial cultures. *Mater. Today: Proc.* **2020**, *12*, 316.
- (33) Kosari, A.; Visser, P.; Tichelaar, F.; et al. Cross-sectional characterization of the conversion layer formed on AA2024-T3 by a lithium-leaching coating. *Appl. Surf. Sci.* **2020**, *512*, No. 145665.
- (34) Li, C.-Y.; Gao, L.; Fan, X.; et al. In vitro degradation and cytocompatibility of a low temperature in-situ grown self-healing Mg-Al LDH coating on MAO-coated magnesium alloy AZ31. *Bioact. Mater.* **2020**, *5*, 364–376.
- (35) Qin, B.; Sheng, Z.; Hao, C.; et al. Superior corrosion and wear resistance of AZ91D Mg alloy via electrodeposited SiO₂-Ni-based composite coating. *Mater. Chem. Phys.* **2022**, *283*, No. 126001, DOI: 10.1016/j.matchemphys.2022.126001.
- (36) Zheng, Z. J.; Gao, Y.; Gui, Y.; et al. Corrosion behavior of nanocrystalline 304 stainless steel prepared by equal channel angular pressing. *Corros. Sci.* **2012**, *54* (1), 60–67, DOI: 10.1016/j.corros.2011.08.049.
- (37) Chen, J.; Wu, L.; Ding, X.; et al. Effects of deformation processes on morphology, microstructure and corrosion resistance of LDH films on magnesium alloy AZ31. *J. Mater. Sci. Technol.* **2021**, *64* (20), 10–20.
- (38) Li, L.-X.; Xie, Z.; Fernandez, C.; et al. Development of a thiophene derivative modified LDH coating for Mg alloy corrosion protection. *Electrochim. Acta* **2020**, *330*, No. 135186.
- (39) Alibakhshi, E.; Ghasemi, E.; Mahdavian, M.; et al. Corrosion inhibitor release from Zn-Al-[PO₄³⁻]-[CO₃²⁻] layered double hydroxides nanoparticles. *Prog. Color Coat.* **2016**, *9*, 233–248.
- (40) Elsener, B.; et al. Impedance Study on the corrosion of PVD and CVD Titanium nitride coatings. *Mater. Sci. Forum* **1989**, *44–45*, 29–38, DOI: 10.4028/www.scientific.net/MSF.44-45.29.
- (41) Matthes, B.; Broszeit, E.; Aromaa, J.; Ronkainen, J.; et al. Corrosion performance of some titanium-based hard coatings. *Surf. Coat. Technol.* **1991**, *49*, 489–495.
- (42) Chaudry, U. M.; Farooq, A.; Tayyab, K.; et al. Corrosion behavior of AZ31 magnesium alloy with calcium addition. *Corros. Sci.* **2022**, *199*, No. 110205.
- (43) van der Weijde, D.; Westing, V.; Wit, D. Electrochemical techniques for delamination studies. *Corros. Sci.* **1994**, *36* (4), 643–652.
- (44) Zhang, K.; Xu, B.; Yang, W.; et al. Halogen-substituted imidazoline derivatives as corrosion inhibitors for mild steel in hydrochloric acid solution. *Corros. Sci.* **2015**, *90*, 284–295.
- (45) Zulkifli, F.; Ail, N.; Yusof, M.; et al. Henna leaves extract as a corrosion inhibitor in acrylic resin coating. *Prog. Org. Coat.* **2017**, *105*, 310–319.
- (46) Ji, G.; Anjum, S.; Sundaram, S.; et al. Musa paradisiac peel extract as green corrosion inhibitor for mild steel in HCl solution. *Corros. Sci.* **2015**, *90*, 107–117.
- (47) Wang, C.; Huang, Y.; Li, J.; et al. Preparation of super-hydrophobic Li-Al-Ala LDH/SA film with enhanced corrosion resistance and mechanical stability on AZ91D Mg alloy. *J. Mater. Sci.* **2022**, *57*, 14780–14798.